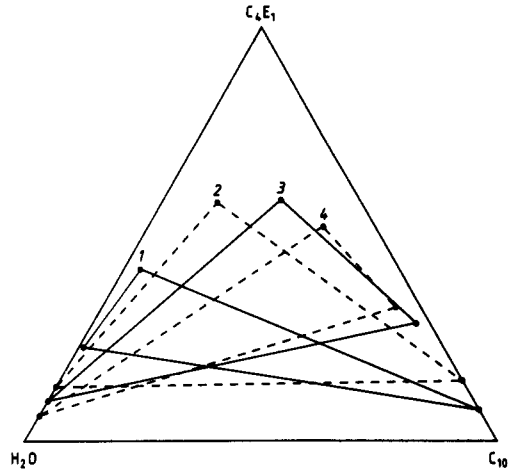

Figure 7. Influence of temperature on the three-phase region in the system $H_2O + C_{10} + C_4E_1$ at $p = 20.0$ MPa: (1) $T = 303.15$ K, (2) $T = 313.15$ K, (3) $T = 323.15$ K, (4) $T = 325.15$ K.

of oil in the middle phase increases, and the solubility of water decreases with increasing temperature.

To verify the accuracy of the experimental results a duplicate measurement was performed at 313.15 K and 30.0 MPa, see Table I. The weight fractions of the three components found in the two experiments show good agreement.

Conclusions

From our measurements it is clear that pressure can play a significant role on the phase behavior of water + oil + nonionic surfactant systems. Furthermore, its influence on the three-phase region can be well understood by the pressure–composition phase prism which we suggested in our earlier work.[18] Vice versa the experimental results found in this study clearly support the suggested phase prism. The most important features of the phase prism are phase transitions of the type $\bar{2}$–3–$\underline{2}$ at constant temperature and increasing pressure. The surfactant-rich middle phase moves with respect to its composition from the oil-rich side of the phase prism to the water-rich side indicating that the surfactant becomes more hydrophilic with increasing pressure. A new experimental setup that enables one to sample the coexisting liquid phase at constant temperature and (elevated) pressure has been used.

Acknowledgment. We are indebted to Mr. K. van der Schoor for technical assistance. We thank Mr. J. H. F. Grondel and Mr. A. van der Plas in assisting us with the design and construction of the equipment. We also thank the "Koninklijke/Shell Exploratie en Produktie Laboratorium", Rijswijk, The Netherlands, for stimulating discussions and financial support.

Registry No. C_{10}, 124-18-5; C_4E_1, 111-76-2.

Molecular Structure of Molybdenum Oxide in Bismuth Molybdates by Raman Spectroscopy

Franklin D. Hardcastle[†] and Israel E. Wachs*

Zettlemoyer Center for Surface Studies, Departments of Chemistry and Chemical Engineering, Lehigh University, Bethlehem, Pennsylvania 18015 *(Received: June 18, 1990; In Final Form: July 19, 1991)*

The Bi_2O_3–MoO_3 system was examined using Raman spectroscopy and a recently developed method for deriving oxygen coordinations and metal–oxygen bond lengths of metal oxide species from their Raman spectra. Many of the compositions examined (Bi:Mo = 2:3–14:1) are multiphasic, consisting of two or more bismuth molybdate phases, as well as a few bismuth oxide phases. The bismuth molybdate phases that occur were found to depend on the Bi:Mo ratio. The following seven bismuth molybdate phases were identified in the Bi:Mo stoichiometeric range from 2:3 to 14:1 α-$Bi_2Mo_3O_{12}$, β-$Bi_2Mo_2O_9$, γ-Bi_2MoO_6, γ'-Bi_2MoO_6 (high-temperature form), $Bi_6Mo_2O_{15}$, $Bi_{37}Mo_7O_{78}$, and a sillenite phase at the 14:1 composition. The complete crystal structures of α-$Bi_2Mo_3O_{12}$, β-$Bi_2Mo_2O_9$, and γ-Bi_2MoO_6 have already been reported in the literature, and the structures of their molybdate species are known. In the present study, the molybdenum coordinations and Mo–O bond lengths are determined for the molybdate species in γ'-Bi_2MoO_6, $Bi_6Mo_2O_{15}$, $Bi_{37}Mo_7O_{78}$, and the sillenite phase. In addition, the bismuth oxide phases are identified for each of the stoichiometries.

I. Introduction

The bismuth molybdates fall into an unusual class of compounds, the ternary bismuth oxide systems Bi–M–O (where M = Mo, W, V, Nb, and Ta), which exhibit a variety of interesting physical properties. For example, the tetragonal phases of thin-film bismuth-derived vanadates, niobates, and tantalates are efficient photoconductors.[1] Thin-film bismuth molybdates have been noted to be effective gas sensors for alcohols and ketones and may be potentially useful as breathalyzer devices.[2] Some of the ternary bismuth oxides show tremendous promise as heterogeneous catalysts.[3] The bismuth molybdates, in fact, are heterogeneous catalysts in commercially important selective oxidations and ammoxidations (the Sohio process): for example, propylene (C_3H_6) to acrolein (C_3H_4O) by oxidation or to acrylonitrile (C_3H_3N) by ammoxidation.[4-7] In spite of the remarkable properties demonstrated by these systems, the molecular structures of many of the phases constituting these important systems are not completely known because of the difficulties encountered in determining the location of the oxygen atoms surrounding the metal sites by diffraction techniques. In light of the importance of these systems, structural studies are currently in progress using a wide assortment

[†] Present address: Sandia National Laboratories, Division 1845, Albuquerque, NM 87185.

(1) Sekiya, T.; Tsuzuki, A.; Torii, Y. *Mater. Res. Bull.* **1985**, *20*, 1383.
(2) Hykaway, N.; Sears, W. M.; Frindt, R. F.; Morrison, S. R. *Sens. Actuators* **1988**, *15*, 105.
(3) Zhou, W.; Jefferson, D. A.; Alario-Franco, M.; Thomas, J. M. *J. Phys. Chem.* **1987**, *91*, 512.
(4) Graselli, R. K.; Burrington, J. D. *Adv. Catal.* **1981**, *30*, 133.
(5) Grasselli, R. K. *J. Chem. Educ.* **1986**, *63*, 216.
(6) Thomas, J. M.; Jefferson, D. A.; Millward, G. R. *JEOL News* **1985**, *23E*, 7.
(7) Jefferson, D. A.; Thomas, J. M.; Uppal, M. K.; Grasselli, R. K. *J. Chem. Soc., Chem. Commun.* **1983**, 594.

0022-3654/91/2095-10763$02.50/0

of structural probes including electron diffraction, high-resolution electron microscopy (HREM), X-ray absorption near-edge structure (XANES), and Raman spectroscopy.[3,8-10] The present study uses Raman spectroscopy to investigate the compositional dependence of the bismuth molybdate and bismuth oxide phases in the stoichiometric range Bi:Mo = 2:3–14:1. The molecular structures of the molybdate species in each of the identified bismuth molybdate phases are determined using a systematic method derived from Raman stretching frequency/bond length/bond strength empirical correlations.

Raman spectroscopy has recently proven to be a very effective tool in the characterization of the structures of transition-metal oxides as bulk phases[11] and two-dimensional surface phases.[12,13] The basic idea behind the conventional method of evaluating Raman spectra is that different molecular structures are expected to have different types of bonds and this, in turn, leads to a different set of Raman spectral features. Used in this way, Raman spectroscopy is an effective structural tool because it can be used to discriminate or "fingerprint" between alternate structures proposed for a chemical species.

Recently, a new, systematic approach[14] has been developed for interpreting the Raman spectra of transition-metal oxides. This approach regards each metal–oxygen bond in a molecular species or crystalline lattice as vibrationally independent of its surroundings so that a direct relationship may be formulated between its metal–oxygen Raman stretching frequencies and bond lengths. Naturally, this approach does not lead to a vibrational mode analysis because it neglects nearest-neighbor interactions and, consequently, bending/wagging and external modes. Furthermore, this approach fails to distinguish between symmetric and antisymmetric stretching modes. Within the limits of experimental error afforded by crystallographic bond length determinations, however, this approach is justified and may be used to determine metal–oxygen bond lengths from Raman stretching frequencies because the effect of the interaction force constants on the bond lengths is smaller than the uncertainty associated with most crystallographic bond length determinations. Applying this reasoning, empirical relations have been established between molybdenum–,[15] vanadium–,[16] niobium–,[17] tungsten–,[18] titanium–,[19] and bismuth–oxygen[9] bond lengths and observed Raman stretching frequencies for reference metal oxide compounds.

In the present study, Raman spectroscopy is used to characterize the molybdenum environments in the bismuth molybdates of compositional range Bi:Mo = 2:3–14:1. The molybdate coordinations and Mo–O bond lengths are determined from the observed Raman stretching frequencies using the stretching frequency/bond length/bond strength empirical relations.[15] In addition, the coexisting bismuth oxide phases are identified by their characteristic Raman bands.

II. Experimental Section

The bismuth molybdates were provided by D. J. Buttrey, D. A. Jefferson, and J. M. Thomas. The bismuth molybdates were prepared by mixing stoichiometric amounts of α-Bi_2O_3 with MoO_3 (both of 99.9% purity), grinding with molar and pestal in a slurry of acetone, followed by drying in air, and finally heating in flowing oxygen at 840 °C.[20]

The Raman spectra were collected by using 10–40 mW of the 514.5-nm line of a Spectra-Physics argon ion laser (Model 171) for excitation. The laser beam power was measured at the sample. The diffusely scattered radiation from the sample was collected in a 90° scattering geometry and directed into a Spex Triplemate spectrometer (Model 1877) coupled to an intensified photodiode array detector (880 intensified array elements) and optical multichannel analyzer (OMA III: Princeton Applied Research, Model 1463). The detector was thermoelectrically cooled to −35 °C. The Raman spectra were collected and recorded with an OMA III (PAR) dedicated computer and software. The spectral resolution and reproducibility were experimentally determined to be better than 2 cm^{-1}. About 100–200 mg of each bismuth molybdate sample was pressed onto a thin layer of KBr to provide mechanical support and pressed into a thin wafer of about 1-mm thickness. The pressed sample was then mounted onto a sample holder capable of spinning at 2000 rpm to avoid local heating effects caused by the concentrated laser beam. Further details concerning the optical arrangement and sample handling procedure used in the Raman experiments can be found elsewhere.[13]

A QUICKBASIC computer program was written to systematically determine every possible combination of Mo–O bond strengths, in valence units, that add to the formal oxidation state of the molybdenum cation according to the valence sum rule.[21,22] The user-input parameters include the formal oxidation state of the molybdenum cation, which is 6.0 vu for the fully oxidized cation, the tolerance on the oxidation state (determined to be 0.12 vu from a previous study),[15] and the observed Raman frequencies greater than about 400 cm^{-1}. The program converts all Raman frequencies to bond strengths, in valence units, and bond lengths in angstroms. The output consists of all possible combinations of bond strengths consistent with the user-input formal oxidation state of the molybdenum cation. Each combination of bond strengths represents a possible molybdate structure, with coordination and bond strengths also provided as output. The "best" molybdate structure is chosen from the list of possible structures according to the following guidelines: (1) The highest occurring Raman stretching frequency must be used, as this represents the shortest Mo–O bond present in the compound. (2) The number of frequencies used must be maximized. After the first two guidelines are followed, (3) the structure(s) with the most consistent valence is chosen, (4) reference structures and information from other structural techniques are used, if possible, and, finally, (5) a hybrid "best" structure is formed from all possible structures not eliminated by using guidelines 1–4. The procedure for forming a hybrid structure is covered in the text. This method of determining the structures of metal oxides from their Raman spectra, which is used in the present study to determine molybdate structures in the bismuth molybdates, has recently been exhaustively covered for several vanadate reference compounds.[16]

III. Theory

The interpretation of the Raman spectrum of a transition-metal oxide species in the solid state is facilitated by imposing two levels of approximation. First, the internal and external modes of the crystal are assumed to be independent of one another. The internal modes of metal oxide molecules within the unit cell of a crystal occur in the medium- and high-frequency regions (>400 cm^{-1} for molybdenum(VI) oxide species) while the external modes, including translational and librational modes, occur at lower frequencies (<400 cm^{-1}). Second, the site symmetry approximation,[23] or correlation method, may be imposed by assigning a high degree

(8) Hardcastle, F. D.; Wachs, I. E.; Eckert, H.; Jefferson, D. A. *J. Solid State Chem.* **1991**, *90*, 194.
(9) Hardcastle, F. D.; Wachs, I. E. *J. Solid State Chem.*, in press.
(10) Hardcastle, F. D.; Wachs, I. E. *J. Solid State Ionics*, submitted for publication.
(11) Nakamoto, K. *Infrared and Raman Spectra of Inorganic and Coordination Compounds*, 3rd ed.; Wiley: New York, 1978.
(12) Dixit, L.; Gerrard, D. L.; Bowley, H. J. *Appl. Spectrosc. Rev.* **1986**, *22*, 189.
(13) Wachs, I. E.; Hardcastle, F. D.; Chan, S. S. *Spectroscopy (Eugene, Oreg.)* **1986**, *1*, 30.
(14) Hardcastle, F. D. Molecular Structures of Bulk and Surface Metal Oxides by Raman Spectroscopy: The Diatomic Approximation. Dissertation, Lehigh University, Bethlehem, PA, 1990; University Microfilms International: Ann Arbor, MI.
(15) Hardcastle, F. D.; Wachs, I. E. *J. Raman Spectrosc.* **1990**, *21*, 683.
(16) Hardcastle, F. D.; Wachs, I. E. *J. Phys. Chem.* **1991**, *95*, 5031.
(17) Hardcastle, F. D.; Wachs, I. E. *Solid State Ionics* **1991**, *45*, 201.
(18) Hardcastle, F. D.; Wachs, I. E. *Chem. Mater.*, submitted for publication.
(19) Hardcastle, F. D.; Peden, C. H. F. *Vib. Spectrosc.*, submitted for publication.
(20) Buttrey, D. J.; Jefferson, D. A.; Thomas, J. M. *Mater. Res. Bull.* **1986**, *21*, 739.
(21) Brown, I. D.; Wu, K. K. *Acta Crystallogr.* **1976**, *32B*, 1957.
(22) Brown, I. D. *Chem. Soc. Rev.* **1978**, *7*, 359.
(23) Fateley, W. G.; Dollish, F. R.; McDevitt, N. T.; Bentley, F. F. *Infrared and Raman Selection Rules for Molecular and Lattice Vibrations: The Correlation Method*; Wiley-Interscience: New York, 1972.

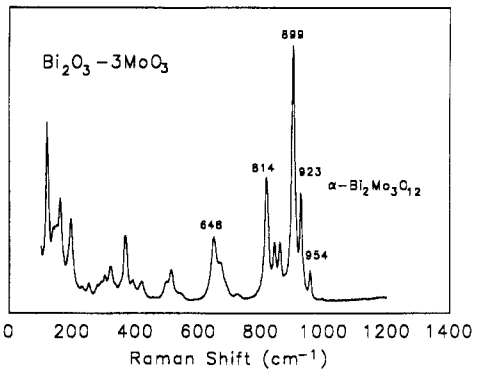

Figure 1. Raman spectrum of Bi_2O_3–$3MoO_3$, showing α-$Bi_2Mo_3O_{12}$ as the only detectable phase.

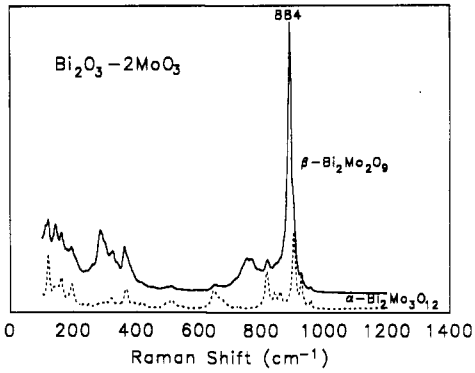

Figure 2. Raman spectrum of Bi_2O_3–$2MoO_3$, showing β-$Bi_2Mo_2O_9$ as the major phase.

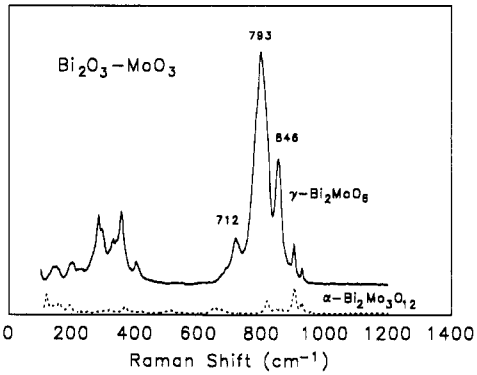

Figure 3. Raman spectrum of Bi_2O_3–MoO_3, showing γ-Bi_2MoO_6 as the major phase.

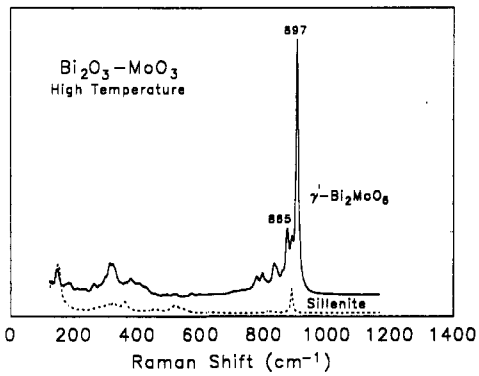

Figure 4. Raman spectrum of the high-temperature form of Bi_2O_3–MoO_3, showing γ'-Bi_2MoO_6 as the major phase.

of symmetry to each atom, or site, within the unit cell. Although the site symmetry approach leads to the total number and types of infrared- and Raman-active modes expected from the crystal, a detailed knowledge of the crystal structure is first required in order to perform the vibrational mode analysis. The site symmetry approach, however, does allow the internal modes of a molecular species confined to a crystalline lattice to be directly compared with those of a similar molecule in solution or the gas phase. Consequently, the site symmetry approach forms the basis of the "fingerprint" method of identifying molecular geometries. For metal oxides with distorted molecular geometries, however, the fingerprint approach cannot be reliably used because of inconsistent matches between spectra due to a virtually infinite number of geometric irregularities possible for a distorted metal oxide species. Clearly, there is a demonstrated need for a systematic way of determining molecular structures from Raman spectra that does not rely on the subjectivity and uncertainty involved with fingerprinting characteristic vibrational bands. Furthermore, the desired systematic method would be generally applicable and capable of yielding detailed structural information not only for ideally symmetric geometries but also for distorted metal oxide species as well.

Recently, empirical relations have been found between the metal–oxygen Raman stretching frequencies and metal–oxygen bond lengths for several transition-metal oxide systems including molybdenum–,[15] vanadium–,[16] niobium–,[17] tungsten–,[18] titanium–,[19] and bismuth–oxygen[9] bonds. In each case, the empirical Raman stretching frequency/bond length relationship was found to follow a simple exponential form. For the present purpose of investigating Mo–O Raman stretching frequencies, the following empirical stretching frequency/bond length relation is used[15]

$$R_{Mo-O} = 0.48239 \ln (32895/\nu) \quad (1)$$

where ν is the Raman stretching frequency in wavenumbers and R is the metal–oxygen bond length in angstroms. Equation 1 yields a standard deviation of $\sigma = 0.016$ Å for a Mo–O bond length.

The Pauling bond strengths of metal–oxygen bonds, in valence units, also referred to as bond orders or bond valences, are useful for discussing the plausibility of proposed metal oxide structures.[21] The Pauling bond strength reflects the relative distribution of available valence electrons throughout the covalent bonds of a metal oxide species. Furthermore, according to the valence sum rule, there is a conservation of valence associated with the metal cation, and this allows the valence sum rule to serve as a bookkeeping device for the number of valence electrons in that structure. Hence, the calculated valence state of the metal cation in a proposed metal oxide structure, arrived at by simply adding the individual metal–oxygen bond valences, may be compared to the formal oxidation state of the metal cation as a simple test for the plausibility of that structure. The empirical expression of Brown and Wu[21] for relating Mo–O bond lengths R to their Pauling bond strengths s is given by

$$s = (R/1.882)^{-6.0} \quad (2)$$

By combining eqs 1 and 2, a relation between the Pauling strength of a Mo–O bond in valence units and its Raman stretching frequency in wavenumbers is expressed as

$$s_{Mo-O} = \{0.256 \ln (32895/\nu)\}^{-6.0} \quad (3)$$

IV. Results

The Raman spectra for the Bi_2O_3–MoO_3 samples, ranging in Bi:Mo composition from 2:3 to 14:1, are presented in Figures 1–6. Most of the bismuth molybdates studied are multiphasic, and this is shown in Table I, which lists the observed Raman bands of the various Bi:Mo compositions with corresponding band positions for each of the identified phases. These phases are briefly summarized in this section.

The molecular structures of the molybdate species in the α-$Bi_2Mo_3O_{12}$, β-$Bi_2Mo_2O_9$, and γ-Bi_2MoO_6 phases have been previously determined by diffraction methods.[24-26] In this section, the crystallographically determined Mo–O bond lengths of these

(24) Van den Elzen, A. F.; Rieck, G. D. *Acta Crystallogr.* **1973**, *29B*, 2433.
(25) Chen, H.; Sleight, A. W. *J. Solid State Chem.* **1986**, *63*, 70.
(26) Teller, R. G.; Brazdil, J. F.; Grasselli, R. K.; Jorgensen, J. D. *Acta Crystallogr.* **1984**, *40C*, 2001.

TABLE I: Summary of the Bi_2O_3–MoO_3 Raman Band Positions

Bi:Mo	phase		band position[a] (cm^{-1})
2:3	α-$Bi_2Mo_3O_{12}$	major	992 (vw), 954 (m), 923 (s), 899 (vs), 856 (m), 838 (m), 814 (s), 720 (w), 685 (vw, sh), 669 (m, sh), 648 (m), 620 (vw, sh), 540 (w), 509 (m), 496 (m, sh), 452 (w), 416 (m), 389 (m), 365 (m), 333 (w), 319 (m), 301 (m), 291 (w, sh), 275 (w, sh), 249 (w), 226 (w), 192 (s), 159 (s), 149 (m, sh), 120 (vs)
1:1	α-$Bi_2Mo_3O_{12}$	minor	953 (w), 922 (w), 896 (m, sh), 854 (w, sh), 836 (w, sh), 814 (m), 716 (w, sh), 669 (vw), 650 (w), 539 (vw), 509 (w), 496 (w), 450 (vw), 413 (w, sh), 365 (w, sh), 191 (w), 160 (m), 121 (m)
	β-$Bi_2Mo_2O_9$	major	884 (vs), 765 (m), 753 (m), 358 (m), 321 (m), 296 (w, sh), 284 (m), 260 (w), 176 (w), 142 (m)
2:1	α-$Bi_2Mo_3O_{12}$	minor	923 (w), 897 (m, sh), 621 (vw), 547 (vw), 509 (vw)
	γ-Bi_2MoO_6	major	846 (s), 793 (vs), 712 (m), 596 (vw), 398 (m), 352 (s), 324 (w), 292 (m, sh), 280 (s), 262 (w, sh), 222 (w), 196 (m), 146 (m)
2:1 (HT)[b]	γ'-Bi_2MoO_6	major	897 (vs), 865 (m), 829 (w, sh), 822 (m), 788 (m), 771 (m), 316 (m), 294 (w, sh), 208 (w)
	sillenite	minor	879 (m), 628 (vw), 514 (w), 359 (w), 142 (s)
	β-Bi_2O_3	minor	450 (vw), 307 (m), 127 (w, sh)
	δ-Bi_2O_3	minor	568 (vw)
3:1	$Bi_6Mo_2O_{15}$	major	880 (vs), 800 (m, br), 359 (m, sh)
	γ'-Bi_2MoO_6	minor	900 (vw), 818 (vw), 788 (vw), 770 (vw), 390 (vw), 360 (vw), 314 (vw)
	β-Bi_2O_3	minor	450 (vw), 294 (s), 147 (vs)
	δ-Bi_2O_3	minor	570 (m, br)
4:1	$Bi_{38}Mo_7O_{78}$	major	870 (vs), 800 (m, br), 330 (w, sh)
	β-Bi_2O_3	minor	450 (w, br), 302 (s), 135 (vs)
	δ-Bi_2O_3	minor	574 (m, br)
38:7	$Bi_{38}Mo_7O_{78}$	major	870 (vs), 801 (m, br), 340 (w, sh)
	β-Bi_2O_3	minor	299 (s), 148 (s, sh)
	δ-Bi_2O_3	minor	563 (m, br)
14:1	sillenite	major	877 (s), 820 (m, sh), 815 (m, sh), 800 (m), 628 (w), 539 (m, sh), 511 (m), 352 (m), 270 (w, sh), 143 (vs), 124 (s)
	α-Bi_2O_3	minor	451 (m), 410 (w), 319 (m), 298 (m, sh), 213 (m), 175 (w, sh)

[a] Key: vw = very weak; w = weak; m = medium; s = strong; vs = very strong; sh = shoulder; br = broad. [b] HT = high-temperature form treated at 645 °C.

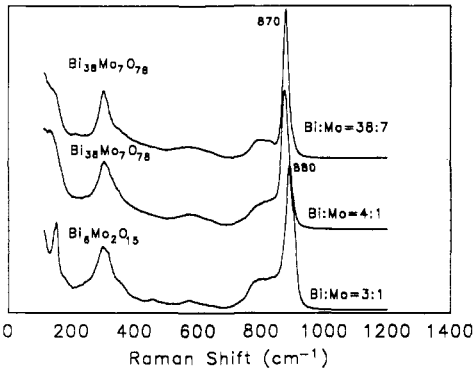

Figure 5. Raman spectrum of (a) $3Bi_2O_3$–$2MoO_3$ (bottom), (b) $2Bi_2O_3$–MoO_3 (middle), and (c) $19Bi_2O_3$–$7MoO_3$ (top).

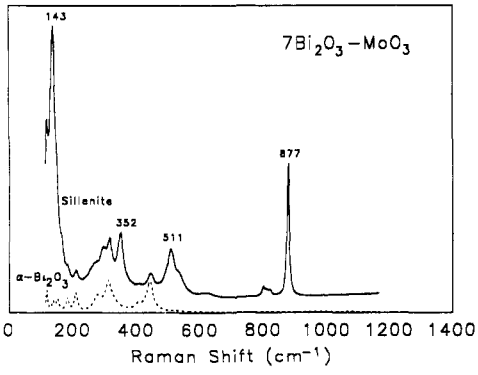

Figure 6. Raman spectrum of $7Bi_2O_3$–MoO_3.

molybdate species are assigned to Raman stretching frequencies by directly comparing their reported bond lengths with their corresponding stretching frequencies. As an exercise, the method of determining the coordinations and Mo–O bond lengths of the molybdate species in these three compounds is first demonstrated on the known structures to illustrate the simplicity and effectiveness of the method. In the Discussion, the same method will be used to determine the coordinations and Mo–O bond lengths of the molybdate species in remaining bismuth molybdate phases having undetermined structures and detected for Bi:Mo compositions of 2:1 (high temperature), 3:1, 4:1, 38:7, and 14:1.

TABLE II: Assigned Raman Frequencies and Mo–O Bond Lengths for α-$Bi_2Mo_3O_{12}$

Mo species (bond length (Å))[a]			assigned Raman freq[b] (cm^{-1})
1	2	3	
1.68			992
	1.69		954
		1.72	923
	1.72		899
		1.73	856
1.78			838
	1.85		814
1.86		1.86	720
1.87			685
		1.89	669
	1.91		648
		2.13	(398)
	2.25		(310)
2.37			(242)

[a] Mo–O bond lengths are from Van den Elzen.[24] [b] Parentheses denote calculated Raman stretching frequencies.

Assigning the Raman Bands of α-$Bi_2Mo_3O_{12}$. The Raman spectrum of the 2:3 composition, Bi_2O_3–$3MoO_3$, is presented in Figure 1 and shows Raman bands due exclusively to the α-$Bi_2Mo_3O_{12}$ phase. This spectrum reveals the high degree of purity of the α-$Bi_2Mo_3O_{12}$ phase at the 2:3 composition because extraneous Raman bands resulting from minor phases are not observed.

Table II shows how the observed Raman stretching modes of the α-$Bi_2Mo_3O_{12}$ phase are assigned by directly correlating the crystallographically determined Mo–O bond lengths with the highest occurring observed Raman bands. Because the structure of α-$Bi_2Mo_3O_{12}$ is reported to have three crystallographically distinct MoO_5 units,[24] the 11 highest occurring observed Raman stretching frequencies, all occuring at greater than 400 cm^{-1}, are assigned to the 10 shortest Mo–O bond lengths of the 3 MoO_5 units in α-$Bi_2Mo_3O_{12}$. The bond lengths and Raman stretching frequencies of α-$Bi_2Mo_3O_{12}$ are assigned in numerical order, with the shortest Mo–O bond of 1.68 Å assigned to the highest occurring band at 992 cm^{-1}, the second shortest Mo–O bond, of 1.69 Å, assigned to the second highest band at 954 cm^{-1}, etc. The longest assigned Mo–O bond, 1.91 Å, is assigned to the band at

TABLE III: α-$Bi_2Mo_3O_{12}$ Structure Determination of Molybdate Species 1 by Raman Spectroscopy

obsd Raman bands (cm^{-1})		Mo–O str	992, 838, 720, 685			
Mo–O bond type		ν	s (vu)		R (Å)	
A		992	1.914		1.689	
B		838	1.443		1.770	
C		720	1.132		1.844	
D		685	1.047		1.867	
poss struct	coordn	A	B	C	D	valence[a]
a	4	1	1	1	1	5.536
b	4	1	1	0	2	5.451
c	4	3	0	0	1	5.376
d	4	0	3	1	0	5.461
e	5	0	0	4	1	5.574
f	5	0	0	3	2	5.489
g	5	0	0	2	3	5.404
best struct			Raman (Å)		lit.[24] (Å)	
a	$1 \times A$		1×1.689 (16)		1×1.68 (1)	
	$1 \times B$		1×1.770 (16)		1×1.78 (1)	
	$1 \times C$		1×1.844 (16)		1×1.86 (1)	
	$1 \times D$		1×1.868 (16)		1×1.87 (1)	
	given		1×2.37 (1)		1×2.37 (1)	

[a] The effective valence of 5.486 vu for the molybdenum cation is determined from the four shortest reported Mo–O bond lengths and the empirical relation of Brown and Wu[21] given by $s = (R/1.882)^{-6.0}$ (see text).

TABLE IV: α-$Bi_2Mo_3O_{12}$ Structure Determination of Molybdate Species 2 by Raman Spectroscopy

obsd Raman bands (cm^{-1})		Mo–O str	954, 899, 814, 648			
Mo–O bond type		ν	s (vu)		R (Å)	
A		954	1.791		1.708	
B		899	1.621		1.736	
C		814	1.376		1.784	
D		648	0.961		1.894	
poss struct	coordn	A	B	C	D	valence[a]
a	4	1	1	1	1	5.749
b	5	1	0	0	4	5.636
c	4	0	2	1	1	5.579
best struct			R (Å)		lit.[24] (Å)	
a	$1 \times A$		1×1.708 (16)		1×1.69 (1)	
	$1 \times B$		1×1.736 (16)		1×1.72 (1)	
	$1 \times C$		1×1.784 (16)		1×1.85 (1)	
	$1 \times D$		1×1.894 (16)		1×1.91 (1)	
	given		1×2.25 (1)		1×2.25 (1)	

[a] The effective valence of 5.647 vu for the molybdenum cation is determined from the four shortest reported Mo–O bond lengths and the empirical relation of Brown and Wu[21] given by $s = (R/1.882)^{-6.0}$ (see text).

648 cm^{-1}. The three longest Mo–O bonds of the MoO_5 units, 2.13, 2.25, and 2.37 Å, are not assigned to Raman bands because they are estimated by eq 1 to stretch at 398, 310, and 242 cm^{-1}, respectively, and would severely overlap with the bending/wagging and external modes (and possible Bi–O stretches) that occur under 400 cm^{-1}. Although these estimated frequencies may be compared to observed frequencies at 389, 301, and 249 cm^{-1}, their actual assignments remain uncertain in view of the variety of vibrational modes expected in the low-frequency region. In order to test the reliability of the Raman band assignments of α-$Bi_2Mo_3O_{12}$ listed in Table II and to illustrate the method of determining the coordination and Mo–O bond lengths from Raman bands, the assigned Raman bands are used to determine the structures of the three molybdate species in this phase by using eqs 1–3 and the resulting bond lengths compared to their literature values.

For simplicity, the longest Mo–O bond length for each of the three MoO_5 units (2.13, 2.25, and 2.37 Å) in α-$Bi_2Mo_3O_{12}$ will be assumed because it is generally not possible to be certain of a band assignment for a Mo–O bond of greater than 2.12 Å (corresponding to about 0.48 vu and 400 cm^{-1}). The QUICKBASIC computer program described in the Experimental Section is used to convert the Raman stretching frequencies to bond lengths and bond strengths by eqs 1 and 3, respectively. Next, the program determines all possible structures consistent with the formal oxidation state of the Mo^{6+} cation within a specified tolerance. In general, for a Mo^{6+} cation this value is 6.0 vu within a tolerance of $\sigma = 0.12$ vu. In the present case, however, because the longest Mo–O bond length in each MoO_5 unit is given, the effective valence accounting for the four remaining Mo–O bonds per Mo^{6+} site is less than 6.0 vu because the valence contribution of the fifth bond is subtracted from this value. According to eq 2, and the Mo–O bond lengths listed in Table II, the calculated valence for the Mo^{6+} cation for each of the three MoO_5 units is determined to be 5.736, 5.989, and 5.897 vu, respectively, for molybdate species 1–3 in α-$Bi_2Mo_3O_{12}$. The valences of the three longest bonds in each of these structures, resulting in respective valences of 0.251, 0.342, and 0.476 vu, are subtracted from the calculated valence state of its corresponding Mo^{6+} cation to yield working valence values of 5.486, 5.647, and 5.421 vu for molybdate species 1–3, respectively.

Table III outlines the systematic procedure for determining the coordination and Mo–O bond lengths of molybdate species 1 (see Table II) in α-$Bi_2Mo_3O_{12}$. The assigned Raman stretching frequencies for the four shortest bonds of the MoO_5 unit (the fifth bond length, 2.37 Å, is assumed) are at 992, 838, 720, and 685 cm^{-1}. As shown in a previous study,[15] each Raman band in the high-frequency region for a molybdate species is assumed to represent a unique Mo–O bond length. Thus, four different bond lengths, labeled A–D in Table III, are initially assumed for molybdate species 1. The QUICKBASIC computer program described in the Experimental Section converts the four Raman stretching frequencies to Pauling bond strengths and bond lengths and then proceeds to find every combination of bond strengths that add to the working valence (see previous paragraph) of 5.489 vu (tolerance $\sigma = 0.12$ vu) for the Mo^{6+} cation. As Table III shows, only seven molybdate structures are possible, labeled a–g, and these are presented along with the coordination, bond types, and calculated Mo^{6+} valence for each structure. Of the seven possible structures, only structure a uses all four Raman stretching frequencies while all other possibilities use less than four frequencies. Thus, as shown at the bottom of Table III, the best structure is (a) with Mo–O bond lengths $1 \times A$, $1 \times B$, $1 \times C$, and $1 \times D$, or 1×1.689 (16), 1×1.770 (16), 1×1.844 (16), and 1×1.868 (16) Å; the fifth Mo–O bond was given as 2.37 (1) Å. Within experimental error, the Mo–O bond lengths are identical to the literature values, also shown at the bottom of Table III.

The identical procedure used in determining the structure of molybdate species 1 in α-$Bi_2Mo_3O_{12}$ is also used to determine the structures of molybdate species 2 and 3, and the results are shown in Tables IV and V. For molybdate species 2, the assigned Raman bands occur at 954, 899, 814, and 648 cm^{-1}, and these four Raman bands give rise to only three possible molybdate structures having a calculated valence of 5.647 vu, within a tolerance of $\sigma = 0.12$ vu, while for molybdate species 3, shown in Table V, eight structures are possible having a calculated valence of 5.421 vu. Clearly, only structure a, for molybdate species 2, and structure c, for molybdate species 3, use the maximum number of four frequencies and are therefore considered to best represent molybdate species 2 and 3, respectively. Both Tables IV and V show that the Raman results compare very well to those of the reported bond lengths determined by diffraction methods. Furthermore, Tables III–V show that Raman spectroscopy is expected to be very effective in the elucidation of coordinations and bond lengths of molybdate species having unknown molecular structures.

The remaining Raman bands above 400 cm^{-1} for α-$Bi_2Mo_3O_{12}$ may be assigned to Bi–O stretches and medium-range order. Although the Raman bands above 600 cm^{-1} for α-$Bi_2Mo_3O_{12}$ are accounted for as Mo–O stretches, and those below 400 cm^{-1} are

TABLE V: α-$Bi_2Mo_3O_{12}$ Structure Determination of Molybdate Species 3 by Raman Spectroscopy

obsd Raman bands (cm^{-1})		Mo–O str	923, 856, 720, 669			
Mo–O bond types		ν	s (vu)		R (Å)	
A		923	1.694		1.724	
B		856	1.494		1.760	
C		720	1.132		1.844	
D		669	1.009		1.879	
poss struct	coordn	A	B	C	D	valence[a]
a	4	2	0	1	1	5.528
b	4	2	0	0	2	5.406
c	4	1	1	1	1	5.329
d	4	1	1	2	0	5.451
e	4	0	3	0	1	5.492
f	5	0	1	0	4	5.532
g	5	0	0	4	1	5.536
h	5	0	0	3	2	5.414
best struct		R (Å)			lit.[24] (Å)	
c	$1 \times A$	1×1.724 (16)			1×1.72 (1)	
	$1 \times B$	1×1.760 (16)			1×1.73 (1)	
	$1 \times C$	1×1.844 (16)			1×1.86 (1)	
	$1 \times D$	1×1.879 (16)			1×1.89 (1)	
	given	1×2.13 (1)			1×2.13 (1)	

[a] The effective valence of 5.421 vu for the molybdenum cation is determined from the four shortest reported Mo–O bond lengths and the empirical relation of Brown and Wu[21] given by $s = (R/1.882)^{-6.0}$ (see text).

assigned collectively as bending/wagging and external modes, the five bands observed at 540, 509, 496, 452, and 416 cm^{-1} (see Table I) were left unassigned. According to a Bi–O stretching frequency/bond length relation,[9] the shortest Bi–O bonds in α-$Bi_2Mo_3O_{12}$, at 2.12 and 2.16 Å, yield estimated Raman frequencies at 452 and 409 cm^{-1}, respectively, and are consistent with the two observed frequencies at 452 and 416 cm^{-1} within the precision of the Bi–O correlation and the crystallographic measurements. The peaks at 540, 509, and 496 cm^{-1}, however, correspond to Bi–O bond lengths of 2.05 (3), 2.07 (3), and 2.08 (3) Å, respectively, and these values are clearly not consistent with the those reported from the X-ray diffraction study.[24] A possible assignment for the bands at 540, 509, and 496 cm^{-1} is that they are due to the stretch of the dioxo Mo_2O_2 linkages connecting pairs of the MoO_4 tetrahedra to form Mo_2O_8 structural units. For example, Griffith[27] has assigned a Raman band at 499 cm^{-1} to the symmetric stretching mode of the Mo_2O_2 dioxo bridge found in $Ba_2(Mo_2O_4(ox)_2(H_2O)_2)$. The dioxo Mo_2O_2 functionality is described as having medium-range order, with its Raman stretching frequency lower than that due to its individual Mo–O bridging bonds and higher than that due to the lattice vibrations characteristic of the long-range order of the crystal lattice.

Assigning the Raman Bands of β-$Bi_2Mo_2O_9$. The Raman spectrum of the 1:1 composition is shown in Figure 2. The 1:1 composition is biphasic, consisting of α-$Bi_2Mo_3O_{12}$, which is present as the minor component and drawn as the dotted line in Figure 2, and β-$Bi_2Mo_2O_9$ which is the major component. The structure of β-$Bi_2Mo_2O_9$ has been reported[25] to consist of four distinct MoO_4 tetrahedra which are slightly distorted and have Mo–O bond lengths ranging from 1.708 to 1.798 Å. It is apparent from Figure 2, however, that these four tetrahedra are not resolved in the Raman spectrum because only three Mo–O stretches are observed at 884, 765, and 753 cm^{-1}.

Table VI shows the structure determination of the molybdate structure in β-$Bi_2Mo_2O_9$ by Raman spectroscopy using a procedure identical to that used for α-$Bi_2Mo_3O_{12}$. Only four structures, a–d, are possible from the three observed Raman bands. Although structures a–c use two frequencies, structure c does not use the highest stretching frequency at 884 cm^{-1} and must therefore be

(27) Griffith, W. P. *J. Chem. Soc. A* **1969**, 211.

TABLE VI: β-$Bi_2Mo_2O_9$ Structure Determination by Raman Spectroscopy

obsd Raman bands (cm^{-1})		Mo–O str	884, 765, 753			
Mo–O bond type		ν	s (vu)		R (Å)	
A		884	1.576		1.745	
B		765	1.246		1.814	
C		753	1.215		1.822	
poss struct	coordn	A	B	C	valence	
a	4	3	1	0	5.973	
b	4	3	0	1	5.942	
c	5	0	1	4	6.104	
d	5	0	0	5	6.073	
best struct		R (Å)			lit.[25] (Å)	
ab	$3 \times A$	1×1.745 (16)	1.758	1.708	1.730	1.717
	$1 \times BC$	1×1.818 (20)	1.763	1.747	1.752	1.759
			1.772	1.747	1.761	1.768
			1.775	1.767	1.798	1.772

rejected (see Experimental Section). A hybrid structure of (a) and (b), which are both MoO_4 tetrahedra, is the best structure because all three observed Raman stretching frequencies are used. The structure of the MoO_4 tetrahedron, as determined from its Raman spectrum with bond lengths of 3×1.745 (16) and 1×1.818 (20) Å, may be compared to those determined by X-ray diffraction where Mo–O bond lengths for the four tetrahedra were found to range from 1.708 (19) to 1.798 (21) Å.

Assigning the Raman Bands of γ-Bi_2MoO_6. The Raman spectrum of the 2:1 composition is shown in Figure 3. The 2:1 composition is biphasic and consists of α-$Bi_2Mo_3O_{12}$, which is the minor component and for which the Raman spectrum is shown as a dotted line in Figure 3, and γ-$BiMoO_6$, which is the major component. The structure of γ-Bi_2MoO_6 has been studied by X-ray diffraction[28] and powder neutron diffraction[26] and found to consist of alternating layers of $Bi_2O_2^{2+}$ and corner-sharing, distorted MoO_6 octahedra (that is, an Aurivillius layered oxide structure). There is one type of MoO_6 octahedron present in this structure, and the observed Raman bands at 846, 793, 712, 596 (very weak), and 398 cm^{-1} are assigned as Mo–O stretching frequencies of the MoO_6 octahedron.

Table VII shows the structure determination of the molybdate species in γ-Bi_2MoO_6 by Raman spectroscopy. There are 23 molybdate structures possible from the 5 observed Raman stretching frequencies, yielding a calculated valence of 6.0 vu (within 0.12 vu), and these are labeled a–w. Only structure n uses all five of the stretching frequencies and is therefore considered to represent the best structure. The bond lengths of this MoO_6 octahedron are $1 \times A$, $1 \times B$, $1 \times C$, $2 \times D$, and $1 \times E$, or 1×1.766 (16), 1×1.797 (16), 1×1.849 (16), 2×1.935 (16), and 1×2.130 (16) Å. As shown at the bottom of Table VIII, this structure is comparable to that determined by diffraction.

Raman Spectra of γ'-Bi_2MoO_6 (High-Temperature Form), $Bi_6Mo_2O_{15}$, $Bi_{38}Mo_7O_{78}$, and Sillenite. The Raman spectrum of the high-temperature modification of the 2:1 composition is presented in Figure 4. The Raman band assignments in Table I show that this sample is multiphasic. The major component is γ'-Bi_2MoO_6, which has been investigated by high-resolution electron diffraction[29] and high-resolution transmission electron microscopy (HRTEM).[30] The oxygen coordination to the Mo and Bi cations in γ'-Bi_2MoO_6, however, has not been reported.

In addition to the γ'-Bi_2MoO_6 phase at the high-temperature 2:1 composition, three additional phases are present as minor components: the sillenite phase, which has the γ-Bi_2O_3 structure and for which the Raman spectrum is shown in Figure 4 as a dotted line, and two polymorphs of bismuth oxide, β-Bi_2O_3 and

(28) Van den Elzen, A. F.; Rieck, G. D. *Acta Crystallogr.* **1973**, *29B*, 2436.

(29) Buttrey, D. J.; Jefferson, D. A.; Thomas, J. M. *Philos. Mag. A* **1986**, *53*, 897.

(30) Watanabe, A.; Horiuchi, S.; Kodama, H. *J. Solid State Chem.* **1987**, *67*, 333.

TABLE VII: γ-Bi_2MoO_6 Structure Determination by Raman Spectroscopy

osbd Raman bands (cm^{-1}) Mo–O str 846, 793, 712, 596, 398

Mo–O bond type	ν	s (vu)	R (Å)
A	846	1.466	1.766
B	793	1.319	1.797
C	712	1.112	1.849
D	596	0.847	1.935
E	398	0.476	2.130

poss struct	coordn	*A*	*B*	*C*	*D*	*E*	valence
a	5	3	0	1	0	1	5.985
b	5	3	0	0	2	0	6.091
c	5	2	2	0	0	1	6.047
d	5	2	1	0	2	0	5.945
e	5	2	0	2	1	0	6.002
f	5	1	3	0	0	1	5.900
g	5	1	2	1	1	0	6.064
h	5	1	0	4	0	0	5.914
i	6	2	1	0	1	2	6.051
j	6	2	0	2	0	2	6.108
k	6	2	0	0	3	1	5.949
l	6	1	2	0	1	2	5.904
m	6	1	1	2	0	2	5.962
n	6	1	1	1	2	1	6.068
o	6	1	0	1	4	0	5.966
p	5	0	3	1	1	0	5.917
q	5	0	2	3	0	0	5.975
r	6	0	3	1	0	2	6.023
s	6	0	2	1	2	1	5.921
t	6	0	2	0	4	0	6.027
u	6	0	1	3	1	1	5.979
v	6	0	1	2	3	0	6.085
w	6	0	0	5	0	1	6.036

best struct		R (Å)	lit.[26] (Å)
n	1 × *A*	1 × 1.766 (16)	1 × 1.75 (1)
	1 × *B*	1 × 1.797 (16)	1 × 1.77 (1)
	1 × *C*	1 × 1.849 (16)	1 × 1.85 (1)
	2 × *D*	2 × 1.935 (16)	1 × 1.86 (1)
	1 × *E*	1 × 2.130 (16)	1 × 2.22 (1)
			1 × 2.28 (1)

δ-Bi_2O_3. β-Bi_2O_3 is metastable but may be observed in its pure form at 650 °C upon cooling from the δ-Bi_2O_3 phase (high-temperature phase) or may be stabilized to room temperature by the addition of small amounts of a metal cation impurity.[31] This phase has been identified by Raman spectroscopy in Ta- and Nb-stabilized structures at a Bi:M = 60:1 composition and has rather sharp, characteristic bands at 462, 311, and 123 cm^{-1}.[9] The presence of β-Bi_2O_3 at the Bi:Mo = 2:1 composition indicates that this phase is stabilized by the molybdenum cation as well, although as only a minor component. As the Bi:Nb or Bi:Ta ratio is decreased from 60:1 to 4:1, the tetragonal lattice of β-Bi_2O_3 transforms to the very complex, cubic lattice of the cation-stabilized δ-Bi_2O_3 phase, which has a very broad Raman band in the 500–600-cm^{-1} region. The Raman bands for the sillenite phase, and the β- and δ-phases of Bi_2O_3 found in the 2:1 sample, are tabulated in Table I.

The Raman spectra for the samples having Bi:Mo compositions of 3:1, 4:1, and 38:7 are shown in Figure 5. These compositions have been investigated by electron diffraction,[20,29,32] but the oxygen coordination around the Mo and Bi cations was not determined. As Table I shows, the 3:1 composition contains a new phase with the stoichiometry $Bi_6Mo_2O_{15}$[29,32] as the major component and γ'-Bi_2MoO_6 as a trace component. As the Bi:Mo ratio is increased to the 4:1 composition, also shown in Figure 5, a new phase of reported[20] stoichiometry $Bi_{38}Mo_7O_{78}$ is present as the major component. The $Bi_{38}Mo_7O_{78}$ phase is most defined at the 38:7 composition, which has a Raman spectrum that is nearly identical to that of the 4:1 composition; the only difference is that the bands

(31) Harwig, H. A. *Z. Anorg. Allg. Chem.* **1978**, *444*, 151.
(32) Miyazawa, S.; Kawana, A.; Koizumi, H.; Iwasaki, H. *Mater. Res. Bull.* **1974**, *9*, 41.

TABLE VIII: γ'-Bi_2MoO_6 Structure Determination by Raman Spectroscopy

obsd Raman bands (cm^{-1}) Mo–O str 897, 865, 829, 822, 788, 771

Mo–O bond types	ν	s (vu)	R (Å)
A	897	1.615	1.738
B	865	1.520	1.755
C	829	1.418	1.776
D	822	1.398	1.780
E	788	1.306	1.800
F	771	1.261	1.811

poss struct	coordn	*A*	*B*	*C*	*D*	*E*	*F*	valence
a	4	2	0	0	1	0	1	5.889
b	4	3	0	0	0	0	1	6.105
c	4	2	1	0	0	0	1	6.011
d	4	2	0	1	0	0	1	5.908
e	4	1	2	0	0	0	1	5.916
f	4	2	0	0	1	1	0	5.934
g	4	2	1	0	0	1	0	6.055
h	4	2	0	1	0	1	0	5.953
i	4	2	0	1	1	0	0	6.045
j	4	2	0	2	0	0	0	6.065
k	4	2	0	0	2	0	0	6.026
l	4	1	2	0	0	1	0	5.961
m	4	1	2	0	1	0	0	6.053
n	4	1	2	1	0	0	0	6.073
o	4	1	1	1	1	0	0	5.951
p	4	1	1	2	0	0	0	5.970
q	4	1	1	0	2	0	0	5.932
r	4	0	3	0	1	0	0	5.959
s	4	0	4	0	0	0	0	6.081
t	4	0	3	1	0	0	0	5.978

best struct		R (Å)
af	2 × *A*	2 × 1.738 (16)
	1 × *D*	1 × 1.780 (16)
	1 × *EF*	1 × 1.805 (21)
t	3 × *B*	3 × 1.755 (16)
	1 × *C*	1 × 1.776 (16)

are much sharper for the 38:7 composition, indicating a more ordered system. The β and δ phases of Bi_2O_3 are present at all three of the Bi:Mo compositions, as shown in Table I.

The Raman spectrum of the sample having a Bi:Mo ratio of 14:1 is shown in Figure 6. This composition is found to contain two phases: The major component is a sillenite phase, and the minor component is the α-Bi_2O_3 phase for which the Raman spectrum is shown in Figure 6 as a dotted line.[33] The α-Bi_2O_3 phase, which possesses a monoclinic lattice,[34] was used as the starting material in the preparations of the bismuth molybdate samples.

V. Discussion

Here, the details of the molybdenum coordination that can be inferred from the interpretation of the Raman data for γ'-Bi_2MoO_6, $Bi_6Mo_2O_{15}$, $Bi_{38}Mo_7O_{78}$, and the distorted sillenite phase are discussed. The molybdenum coordination in these bismuth molybdate phases has previously not been determined.

Structure Determination of γ'-Bi_2MoO_6 (High-Temperature Form) by Raman Spectroscopy. The perovskite γ-Bi_2MoO_6 transforms to γ'-Bi_2MoO_6 when heated to 645 °C. As noted before, the structure of γ'-Bi_2MoO_6 has been investigated by high-resolution transmission electron microscopy.[29,30] These studies showed a structural relationship between fluorite and γ'-Bi_2MoO_6. The space group of γ'-Bi_2MoO_6 was determined to be $P2_1/c$ with lattice parameters a = 17.244 (1) Å, b = 22.420 (2) Å, c = 5.5857 (6) Å, and β = 90.486 (7)°, with 16 formula units per unit cell.

Previous investigations have resulted in a number of proposed structures for the molybdenum and bismuth oxide polyhedra in the γ'-Bi_2MoO_6 phase. Electron diffraction work led by Buttrey[29]

(33) Betsch, R. J.; White, W. B. *Spectrochim. Acta* **1978**, *34A*, 505.
(34) Malmros, G. *Acta Chem. Scand.* **1970**, *24*, 384.

suggested a structure similar to that of β-$Bi_2Mo_2O_9$ where columns of isolated MoO_4 tetrahedra form square tunnels enclosing a single column of Bi^{3+} sites. These square tunnels are arranged in pairs and are further linked by additional MoO_4 tetrahedra. Watanabe[30] proposed that each Mo^{6+} cation is surrounded by four oxygen atoms at 1.9 Å with the possible presence of a MoO_5 unit. Matsuura[35] found the Raman spectrum of γ'-Bi_2MoO_6 to be similar to that of α-$Bi_2Mo_3O_{12}$ and consequently proposed the presence of at least three different MoO_4 configurations in γ'-Bi_2MoO_6 because of the three types of molybdate species present in the α-$Bi_2Mo_3O_{12}$ structure.

The presence of an isolated MoO_4 tetrahedron in γ'-Bi_2MoO_6 is indicated by the absence of Mo–O stretching bands in the 730–540-cm^{-1} region of the spectrum in Figure 4. This is because MoO_6 octahedra and bridged structures (that is, having Mo–O–Mo linkages) possess Mo–O bonds of about unit valency and the Mo–O stretching frequencies associated with these bonds occur in the 730–540-cm^{-1} region. For example, compounds having distorted MoO_6 units display bands in this region as shown: $CoMoO_4$, 943, 694 cm^{-1}; $NiMoO_4$, 966, 914, 701 cm^{-1}; MoO_3, 997, 820, 660 cm^{-1}; $(NH_4)_6Mo_7O_{24}\cdot 4H_2O$, 934, 893, 888, 633, 625, 570, 543 cm^{-1}; $(NH_4)_2Mo_2O_7$, 910, 843, 694 cm^{-1}.[15] By comparison, γ-Bi_2MoO_6 has a more regular MoO_6 octahedron with Raman bands at 846, 792, and 712 cm^{-1} (see Table I). In short, the absence of Raman bands in the 730–540-cm^{-1} region argues against MoO_6 as well as bridged MoO_5 and MoO_4 species. This lack of evidence for Mo–O–Mo linkages provides strong evidence for the presence of isolated MoO_4 tetrahedra in the γ'-Bi_2MoO_6 structure. Further evidence is provided by the characteristic position of the highest frequency band at 897 cm^{-1} which is consistent with that of a slightly distorted, isolated MoO_4 tetrahedron. For example, $Na_2MoO_4\cdot 2H_2O$ and $Bi_3(FeO_4)(MoO_4)_2$ both have slightly distorted MoO_4 tetrahedra, and each shows a Raman Mo–O stretching band at 897 cm^{-1}.[15] From these combined observations it is concluded that the γ'-Bi_2MoO_6 structure contains slightly distorted and isolated MoO_4 tetrahedra. This conclusion is in agreement with recent findings using X-ray absorption near-edge structure spectroscopy.[36]

The structure determination of the molybdate species in γ'-Bi_2MoO_6 is shown in Table VIII. Six Mo–O stretching frequencies are observed at 897, 865, 829, 822, 788, and 771 cm^{-1}, and these give rise to 20 possible molybdate structures, labeled a–t; note that all structural possibilities are MoO_4 tetrahedra. There must be more than one type of MoO_4 tetrahedron in the γ'-Bi_2MoO_6 structure because there are more than four distinct Raman Mo–O stretching frequencies and, consequently, more than four different bond types. If two distinct MoO_4 tetrahedra are present, then the shortest Mo–O bond in each structure would exhibit a unique highest occurring stretching frequency that would occur above 858 cm^{-1} (which is the Raman stretching frequency estimated for a perfect MoO_4 tetrahedron).[15] Accordingly, the very sharp Raman band observed at 865 cm^{-1} (see Figure 4) is assigned to the shortest Mo–O bond of the second MoO_4 tetrahedron in the γ'-Bi_2MoO_6 structure. The best combination of structural possibilities consistent with the presence of two unique MoO_4 tetrahedra is a hybrid of structures a and f representing the first tetrahedron and structure t representing the second tetrahedron. Thus, the first MoO_4 tetrahedron in γ'-Bi_2MoO_6 has bond lengths of $2 \times A$, $1 \times D$, and $1 \times EF$, or 2×1.738 (16), 1×1.780 (16), and 1×1.805 (21) Å. The second MoO_4 tetrahedron in γ'-Bi_2MoO_6 is very regular with bond lengths of $3 \times B$ and $1 \times C$, or 3×1.755 (16) and 1×1.776 (16) Å. These results are summarized in Table VIII.

The structures of the molybdate species in γ'-Bi_2MoO_6, as determined in the present Raman study, may be compared to previously proposed models. Matsuura[35] compared the Raman spectrum of γ'-Bi_2MoO_6 to that of α-$Bi_2Mo_3O_{12}$ and subsequently proposed at least three different MoO_4 configurations in γ'-Bi_2MoO_6. A visual inspection of the Raman spectra of α-$Bi_2Mo_3O_{12}$ and γ'-Bi_2MoO_6 in Figures 1 and 4, however, shows that the Raman features of these two phases are dramatically different: α-$Bi_2Mo_3O_{12}$ has Raman bands as high as 953 cm^{-1} for nonbridging Mo–O bonds and several bands in the 500–750-cm^{-1} region due to bridging Mo–O bonds, whereas γ'-Bi_2MoO_6 exhibits stretching modes only in the 897–771-cm^{-1} region. In fact, the Raman features of γ'-Bi_2MoO_6 more closely resemble those of β-$Bi_2Mo_2O_9$, which has Mo–O stretching modes in the 884–753-cm^{-1} region (see Tables I and VI). Watanabe's[30] proposal of MoO_4 units with Mo–O bond lengths at 1.9 Å (calculated Mo^{6+} valence of 3.8 vu by eq 2 indicating erroneous bond lengths) is similar to the present study except that in the present study the tetrahedra were found to have bond lengths ranging from 1.74 to 1.80 Å in one tetrahedron and 1.76 to 1.78 Å in the other tetrahedron. The model that is perhaps most consistent with the results of the present study is from the electron diffraction work of Buttrey[29] in which two types of MoO_4 tetrahedra were proposed: isolated MoO_4 tetrahedra forming square tunnels and enclosing a single column of Bi^{3+} sites and a second type of MoO_4 tetrahedron linking pairs of these tunnels.

Structure Determination of $Bi_6Mo_2O_{15}$ and $Bi_{38}Mo_7O_{78}$ by Raman Spectroscopy. The $Bi_6Mo_2O_{15}$ phase, which is present only at the 3:1 composition, was determined to have a defect fluorite structure and a space group of $P2/c$.[29,32] The lattice parameters were determined to be $a = 24.786$ Å, $b = 5.805$ Å, $c = 23.527$ Å, and $\beta = 102.93°$ with 9 formula units per unit cell. The structure of the molybdate species was not determined. The Raman spectrum of the $Bi_6Mo_2O_{15}$ phase (Figure 5) shows bands at 880 and 800 cm^{-1}, which are assigned to the Mo–O stretching vibrations of a MoO_4 tetrahedron because of the very close similarity of its Raman features to those of β-$Bi_2Mo_2O_9$ (Figure 2) and γ'-Bi_2MoO_6 (Figure 4).

The $Bi_{38}Mo_7O_{78}$ phase dominates at both the 4:1 and 38:7 compositions. The structure of $Bi_{38}Mo_7O_{78}$ was determined by X-ray microanalysis and electron and X-ray powder diffraction to have a $3 \times 5 \times 3$ fluorite superlattice.[20] Its orthorhombic space group is $Pccn$, with lattice parameters $a = 16.818$ Å, $b = 28.658$ Å, and $c = 16.903$ Å, with 4 formula units per unit cell. The structure of the molybdate species was not determined. The Raman spectrum of the $Bi_{38}Mo_7O_{78}$ phase closely resembles that of the $Bi_6Mo_2O_{15}$ phase; the only difference is that the highest frequency band at 880 cm^{-1} for $Bi_6Mo_2O_{15}$ is shifted down by 10 cm^{-1} to 870 cm^{-1} for $Bi_{38}Mo_7O_{78}$, indicating a slightly more regular MoO_4 tetrahedron for the $Bi_{38}Mo_7O_{78}$ phase.

The structure determination of the molybdate species in $Bi_6Mo_2O_{15}$ and $Bi_{38}Mo_7O_{78}$ by Raman spectroscopy is shown in Table IX. Each phase exhibits only two Mo–O stretching modes: 880 and 800 cm^{-1} for $Bi_6Mo_2O_{15}$ and 870 and 800 cm^{-1} for $Bi_{38}Mo_7O_{78}$. As Table IX shows, only one structure is possible for each set of bands. The resulting bond lengths for the MoO_4 tetrahedron in $Bi_6Mo_2O_{15}$ are $3 \times A$ and $1 \times B$, or 3×1.747 (16) and 1×1.793 (16) Å, while the bond lengths for the tetrahedron in $Bi_{38}Mo_7O_{78}$ are 3×1.752 (16) and 1×1.793 (16) Å. Thus, the molybdate tetrahedra in both $Bi_6Mo_2O_{15}$ and $Bi_{38}Mo_7O_{78}$ are found to have identical bond lengths within experimental error.

Structure of the Sillenite Phase by Raman Spectroscopy. Buttrey[29] has noted that no new phases are detected upon increasing the Bi:Mo ratio above 38:7, where the $Bi_{38}Mo_7O_{78}$ phase dominates. He further noted that there may be a partial solubility between $Bi_{38}Mo_7O_{78}$ and Bi_2O_3 (phase not specified) at higher Bi:Mo compositions. In contrast to these results, the Raman spectrum of the 14:1 composition, shown in Figure 6, does not show the presence of $Bi_{38}Mo_7O_{78}$. Instead, Raman bands are observed for the α-Bi_2O_3 phase, which is used as the starting material in the preparations of the bismuth molybdates, and characteristic Raman bands are noted for the sillenite phase which is present as the major component at the 14:1 composition. The characteristic Raman bands for both of these phases are listed in Table I. A description of the sillenite structure is given in the following paragraph.

The sillenite structure, which in the present study is a Mo-doped Bi_2O_3 phase, is believed to be isomorphous with pure γ-Bi_2O_3,

(35) Matsuura, I.; Schut, R.; Hirakawa, K. *J. Catal.* **1980**, *63*, 152.
(36) Wong, J. Private communication.

TABLE IX: $Bi_6Mo_2O_{15}$ and $Bi_{38}Mo_7O_{78}$ Structure Determination by Raman Spectroscopy

$Bi_6Mo_2O_{15}$

obsd Raman bands (cm^{-1})		Mo–O str		880, 800
Mo–O bond type	ν	s (vu)		R (Å)
A	880	1.564		1.747
B	800	1.338		1.793
poss struct	coordn	A	B	valence
a	4	3	1	6.030
best struct				R (Å)
a	$3 \times A$			3×1.747 (16)
	$1 \times B$			1×1.793 (16)

$Bi_{38}Mo_7O_{78}$

obsd Raman bands (cm^{-1})		Mo–O str		870, 800
Mo–O bond type	ν	s (vu)		R (Å)
A	870	1.535		1.752
B	800	1.338		1.793
poss struct	coordn	A	B	valence
a	4	3	1	5.942
best struct				R (Å)
a	$3 \times A$			3×1.752 (16)
	$1 \times B$			1×1.793 (16)

which is metastable and forms at 639 °C by cooling from the high-temperature form of bismuth oxide, δ-Bi_2O_3.[31] At lower temperatures, the γ-Bi_2O_3 structure is stabilized by a metal cation impurity, thereby yielding the sillenite structure. The most ideal sillenite structures are those containing quadrivalent metal cations such as Si^{4+} and Ge^{4+} to form $Bi_{12}SiO_{20}$ and $Bi_{12}GeO_{20}$.[37] The metal cations themselves occupy nearly perfect tetrahedral sites in the sillenite structure, giving rise, for example, to nearly perfect SiO_4 or GeO_4 tetrahedra. The sillenite structure has also been stabilized by pentavalent cations such as P^{5+}, As^{5+}, V^{5+}, and Bi^{5+} and the Raman spectra of these compounds have been reported.[38]

The formation of the sillenite structure at the 14:1 composition in the Bi–Mo–O system is unexpected in view of the reports in the literature that hexavalent metal cations such as Mo^{6+} and W^{6+} do not stabilize the sillenite structure.[39] Although the Raman spectrum of the 14:1 composition (Figure 6) clearly shows characteristic bands for the sillenite structure (see Table I for tabulation), the bands are slightly broader than those reported for quadrivalent- and pentavalent-stabilized sillenite structures such as $Bi_{12}SiO_{20}$[37] and $Bi_{25}VO_{40}$,[8] indicating a more disordered bismuth oxide lattice. Furthermore, the Raman Bi–O stretching frequencies of the Bi–Mo–O sillenite structure are shifted in wavenumber from those of the Bi–Si–O and Bi–V–O sillenite structures, indicating a slightly different set of Bi–O bond lengths. A comparison of the Raman frequencies of $Bi_{12}SiO_{20}$ with those of the 14:1 composition shows the following shifts for the Bi–O vibrational modes: 619 to 628 cm^{-1}, 530 to 539 cm^{-1}, 448 to 511 cm^{-1}, 321 to 352 cm^{-1}, and 267 to 270 cm^{-1} for $Bi_{12}SiO_{20}$ and Bi:Mo = 14:1, respectively. These Raman band shifts for the Bi–O modes of the sillenite structure, however, are commonly observed as the oxidation state of the stabilizing metal cation is altered from 4+ to 5+.[38]

In contrast to the Raman bands of the bismuth oxide structure in Figure 6, the Raman bands of the MoO_4 tetrahedron in the sillenite structure are very sharp, indicating a very regular structure for this molybdate species. The perfect MoO_4 tetrahedron has been estimated to have an Mo–O Raman stretch at 858 cm^{-1}, with a precision of $\sigma \simeq 25$ cm^{-1}, and the observed value of 877 cm^{-1} for the tetrahedron in the 14:1 composition is consistent with this value within the reported experimental error of the Mo–O stretching frequency/bond length correlation.[15] By analogy to molybdate reference compounds, the MoO_4 tetrahedron in the sillenite structure is comparable to that found in $CaMoO_4$, which has reported Mo–O bond lengths of 1.775 Å[40] and Raman stretching modes at 879 (most intense), 848, and 794 cm^{-1}.[41]

TABLE X: Sillenite Phase Structure Determination of the Molybdate Species by Raman Spectroscopy

obsd Raman bands (cm^{-1})		Mo–O str				877, 820, 815, 800
Mo–O bond type	ν		s (vu)			R (Å)
A	877		1.555			1.748
B	820		1.393			1.781
C	815		1.379			1.784
D	800		1.338			1.793
poss struct	coordn	A	B	C	D	valence
a	4	3	0	0	1	6.004
b	4	3	1	0	0	6.058
c	4	3	0	1	0	6.045
d	4	2	2	0	0	5.896
e	4	2	1	1	0	5.882
best struct						R (Å)
ae		$2 \times A$				2×1.748 (16)
		$1 \times AB$				1×1.765 (32)
		$1 \times CD$				1×1.788 (20)

The structure determination of the molybdate species in the sillenite phase by Raman spectroscopy is shown in Table X. Four stretching frequencies are identified in the high-frequency region at 877, 820, 815, and 800 cm^{-1}, and all are assigned as Mo–O stretching frequencies. As Table X shows, only five molybdate structures are possible from these stretching frequencies and all are MoO_4 tetrahedra. Structure e uses three frequencies while structures a–d each use only two frequencies. In order to use all four observed Raman stretching frequencies, however, a hybrid structure is formed from structures a and e. This results in Mo–O bond lengths of $2 \times A$, $1 \times AB$, and $1 \times CD$, or 2×1.748 (16), 1×1.765 (32), and 1×1.788 (20) Å, for the MoO_4 tetrahedron in the sillenite structure.

VI. Conclusions

The Bi_2O_3-MoO_3 system was examined with Raman spectroscopy. Seven distinct molybdenum-containing phases and four bismuth oxide phases were identified and the compositional regions of their existence established. In addition to detecting the phases present at each Bi:Mo composition, the Raman spectra permitted the structural determination of the molybdate species in these phases. The crystal structures of the α-$Bi_2Mo_3O_{12}$, β-$Bi_2Mo_2O_9$, and γ-Bi_2MoO_6 phases are known, and this allowed the assignment of their Mo–O bond lengths to their Raman stretching frequencies. In contrast, the molecular structures in the molybdate phases γ'-Bi_2MoO_6, $Bi_6Mo_2O_{15}$, $Bi_{38}Mo_7O_{78}$, and a Bi–Mo–O sillenite phase have not been reported. In the present study, the molecular structures of the molybdate species in these undetermined bismuth molybdate phases were determined by Raman spectroscopy using a new, systematic method that takes advantage of previously determined Raman stretching frequency/bond length/bond strength empirical correlations.

All four of the new bismuth molybdate phases investigated contain regular, isolated MoO_4 tetrahedra. At the Bi:Mo = 2:1 composition (treated at 645 °C), γ'-Bi_2MoO_6 is the major phase and was found to contain two types of MoO_4 tetrahedra: one slightly distorted with bond lengths of 2×1.738 (16), 1×1.780 (16), and 1×1.805 (21) Å and a very regular tetrahedron with bond lengths of 3×1.755 (16) and 1×1.776 (16) Å. At the

(37) Abrahams, S. C.; Jamieson, P. B.; Bernstein, J. L. *J. Chem. Phys.* **1967**, *47*, 4034.
(38) Devalette, M.; Darriet, J.; Couzi, M.; Mazeau, C.; Hagenmuller, P. *J. Solid State Chem.* **1982**, *43*, 45.
(39) Kargin, Y. F.; Mar'in, A. A.; Skorikov, V. M. *Izv. Akad. Nauk SSSR, Neorg. Mater.* **1982**, *18*, 1605.
(40) Wandahl, G.; Christensen, A. N. *Acta Chem. Scand.* **1987**, *41A*, 358.
(41) Liegeois-Duyckaerts, M.; Tarte, P. *Spectrochim. Acta* **1972**, *28A*, 2037.

3:1 composition, $Bi_6Mo_2O_{15}$ predominates and has a MoO_4 tetrahedron with bond lengths of 3 × 1.747 (16) and 1 × 1.793 (16) Å. At the 4:1 and 38:7 compositions, the major phase is $Bi_{38}Mo_7O_{78}$ and its MoO_4 tetrahedron is essentially identical to that in $Bi_6Mo_2O_{15}$ with bond lengths of 3 × 1.752 (16) and 1 × 1.793 (16) Å. At the 14:1 composition, the molybdenum-stabilized sillenite structure is the major phase and its MoO_4 tetrahedron has bond lengths of 2 × 1.748 (16), 1 × 1.765 (32), and 1 × 1.788 (20) Å.

The systematic method used in the present study for interpreting the Raman spectra of molybdate species by using empirical Raman stretching frequency/bond length/bond strength relations is a very effective way of determining the coordinations and bond lengths of molybdate species from their Raman spectra. In cases where diffraction techniques fall short of providing the oxygen positions around cations in a metal oxide system, Raman spectroscopy may be used to generate this vital structural information. Used in this way, Raman spectroscopy becomes an important complementary technique to diffraction methods in structural investigations of transition-metal oxide systems.

Acknowledgment. We are indebted to D. A. Jefferson (University of Cambridge), D. A. Buttrey (University of Delaware), and J. M. Thomas (The Royal Institute) for supplying the bismuth molybdate samples. Financial support from the Texaco Philanthropic Foundation and the Sherman Fairchild Foundation is acknowledged by F.D.H.

Registry No. Bi_2O_3, 1304-76-3; MoO_3, 1313-27-5; α-$Bi_2Mo_3O_{12}$, 13595-85-2; β-$Bi_2Mo_2O_9$, 16229-40-6; γ-Bi_2MoO_6, 13565-96-3; $Bi_6Mo_2O_{15}$, 51682-19-0; $Bi_{38}Mo_7O_{78}$, 103715-01-1.

Site Group Analysis of Normal Modes in Semiconductor Superlattices

B. H. Bairamov, R. A. Evarestov, Yu. E. Kitaev,

A. F. Ioffe Physical-Technical Institute, St. Petersburg 194021, USSR

E. Jahne,*

Zentralinstitut fuer Elektronenphysik, Berlin 1086, Germany

M. Delaney, T. A. Gant,† M. V. Klein, D. Levi, J. Klem,‡,§ and H. Morkoc‡

Department of Physics and Materials Research Laboratory, University of Illinois at Urbana-Champaign (UIUC), 110 W. Green Street, Urbana, Illinois 61801 *(Received: November 12, 1990; In Final Form: June 25, 1991)*

We present a site group analysis of normal modes in semiconductor superlattices which permits us to connect by symmetry the local atomic displacements and normal vibrational modes over the entire Brillouin zone. The arrangements of atoms over the Wyckoff positions for $(GaAs)_m(AlAs)_n$ and $(Si)_m(Ge)_n$ superlattices oriented along [001] are determined for different sets of m and n. We obtain the symmetry for $k \neq 0$ phonons using the theory of the band respresentations of space groups and derive selection rules for one- and two-phonon infrared absorption and for first- and second-order Raman scattering. Raman spectra are presented for $(GaAs)_7(AlAs)_{18}$ and $(Si)_3(Ge)_3$ superlattices and interpreted in terms of the elaborated theory.

1. Introduction

New techniques allow the fabrication of rather complex crystals with a large number of atoms in the primitive cell. Success in growing $(GaAs)_m(AlAs)_n$ and $(Si)_m(Ge)_n$ superlattices (SL's) with varying primitive cell, consisting of m and n monolayers of GaAs and AlAs (Si and Ge), respectively, by molecular beam epitaxy as well as characterization by Raman scattering of these SL's has been demonstrated recently by several groups.[1-20] Improvements in growth techniques and growth control give the ability to produce ultrathin high-quality SL's with period $(m + n)d_0$ (d_0 being an interatomic spacing) comparable or even less than the de Broglie wavelength of electrons. In such short-period SL's, quantum size effects with tailored band gaps can be observed.

In the case of $(Si)_m(Ge)_n$ SL's, there is a built-in asymmetrically distributed strain due to the large lattice mismatch (~4.2%), although the Si and Ge surfaces are chemically similar and bonded perfectly. Symmetrization of strain of short-period $(Si)_m(Ge)_n$ SL's was achieved very recently by incorporation of a thin homogeneous $Si_{1-x}Ge_x$ buffer layer of an appropriate thickness and composition.[13] Due to the new periodicity and folding of the Brillouin zone (BZ) the most interesting phenomenon in symmetrically strained $(Si)_m(Ge)_n$ SL's is the band-gap conversion

† Present address: Division of Physics, National Research Council, Ottawa K1a0R6, Canada.

‡ Coordinated Science Laboratory, UIUC.

§ Present address: Sandia National Laboratory, Albuquerque, NM 87185-5800.

(1) Klein, M. V. *IEEE J. Quantum Electron.* **1986**, *QE-22*, 1760.
(2) Jusserand, B.; Cardona, M. *Light Scattering in Solids*; Cardona, M., Güntherodt, G., Eds.; Springer Verlag: Heidelberg, 1989; Vol. V, p 49.
(3) Bairamov, B. H.; Evarestov, R. A.; Ipatova, I. P.; Kitaev, Yu. E.; Maslov, A. Yu.; Delaney, M.; Gant, T. A.; Klein, M. V.; Levi, D.; Klem, J.; Morkoc, H. Proceedings of the Fourth Interational Conference on Superlattices, Microstructures and Microdevices, Trieste, 1988. *Superlattices Microstruct.* **1989**, *6*, 227.
(4) Wang, Z. P.; Han, H. X.; Li, G. H.; Jiang, D. S.; Ploog, K. *Phys. Rev.* **1988**, *B38*, 8483.
(5) Fasol, G.; Tanaka, M.; Sakaki, H.; Hirokoshi, Y. *Phys. Rev.* **1988**, *B38*, 6056.
(6) Brigger, H.; Abstreiter, G.; Jorke, H.; Herzog, H. J.; Kasper, E. *Phys. Rev.* **1986**, *B33*, 5928.
(7) Dharma-wardana, M. W. C.; Lockwood, D. J.; Baribeau, J. M.; Houghton, D. C. *Phys. Rev.* **1986**, *B34*, 3034.
(8) Ospelt, M.; Bacsa, W.; Henz, J.; Mäder, K. A.; Känel, H. von. *Superlattices Microstruct.* **1988**, *4*, 717.
(9) Menẽndez, J.; Pinczuk, A.; Bevk, J.; Mannaerts, J. *J. Vac. Sci. Technol.* **1988**, *B6*, 1306.
(10) Alonso, M. I.; Cardona, M.; Kanellis, G *Solid State Commun.* **1989**, *69*, 479; Corrigendum **1989**, *69*, 70(7).
(11) Fasolino, A.; Molinari, E. *J. Phys. (Paris)* **1987**, *C5*, 569.
(12) Alonso, M. A.; Cerdeira, F.; Niles, D.; Cardona, M. *Appl. Phys. Lett.* **1989**, *55*, 411.
(13) Kasper, E.; Kibbel, H.; Jorke, H.; Brügger, H.; Friess, E.; Abstreiter, G. *Phys. Rev.* **1988**, *B38*, 3599.

0022-3654/91/2095-10772$02.50/0